Stabilizing explicit $\omega - x$ migration using local WKBJ operators

Chad M. Hogan, Gary F. Margrave

ABSTRACT

A new operator for the GPSPI migration algorithm is introduced. It is shown that a suitably chosen vertical velocity profile $v(z)$ with a linear positive gradient limits a point source at depth so that the entire upper hemisphere of its wavefront reaches the surface within a finite aperture. This concept is used to design a WKBJ operator. The resulting operator is shown to have a finite aperture and is stable when localized.

INTRODUCTION

Recursive phase-shift wavefield propagation

Many current wavefield extrapolation migration algorithms are space-frequency methods related to or derived from the phase-shift method introduced by Gazdag (1978). Fourier-transforming the scalar wave equation results in the Helmholtz equation, which results in an interpretation of the wavefield as a sum of plane waves. By applying an appropriate phase-shift to each plane wave, the wavefield may be propagated through a distance accurately.

Generalized PSPI

The generalized phase-shift plus interpolation (GPSPI) algorithm described by Margrave and Ferguson (1999) is an accurate, efficient implementation of these phase-shift concepts. This algorithm takes an entire constant-depth-slice of the wavefield and propagates it to a deeper level. The z (depth) direction is typically referred to as the *range* direction, while horizontal directions x and sometimes y are referred to as *transverse* directions. In addition to Fourier-transforming the time series of the data, it is often convenient to represent the transverse directions x and y in their Fourier-transformed coordinates, k_x and k_y.

Mathematically, the GPSPI algorithm may be represented in compact operator notation as:

$$\Psi(x, z = \Delta z, \omega) = \mathbf{T}_\alpha \Psi(x, z = 0, \omega) \tag{1}$$

Or, more explicitly:

$$\Psi(x, z = \Delta z, \omega) \approx \int_{\mathbb{R}} \phi(k_x, z = 0, \omega) \alpha\left(k\left(x\right), k_x, \omega\right) e^{ik_x x} dk_x \tag{2}$$

where

$$\alpha\left(k\left(x\right), k_x, \omega\right) = \begin{cases} e^{i\Delta z k_z(x)}, |k_x| \leq \frac{\omega}{v(x)} \\ e^{-|\Delta z k_z(x)|}, |k_x| > \frac{\omega}{v(x)} \end{cases}, \qquad \begin{aligned} k_z(x) &= \sqrt{k(x)^2 - k_x^2} \\ k(x) &= \tfrac{\omega}{v(x)} \end{aligned} \tag{3}$$

and

$$\phi(k_x, z = 0, w) = \frac{1}{2\pi} \int_{\mathbb{R}} \Psi(x, z = 0, \omega) e^{-ik_x x} dx \tag{4}$$

The algorithm applies a nonstationary filter to the data (Margrave, 1998), is a pseudodifferential operator in the Standard Calculus (Hörmander, 1985) and is the limiting form of the PSPI algorithm described by Gazdag and Sguazzero (1984) when taken to the extreme of using a separate velocity for each and every output point. (Margrave and Ferguson, 1999). In the pseudodifferential calculus, α is known as the symbol of the operator $\mathbf{T}_\alpha$, which is explicitly defined in equation (2).

It may be seen that the wavefield $\Psi(x, z, \omega)$ at each output point $(x_0, \Delta z)$ is the result of the wavefield extrapolation operator $\mathbf{T}_\alpha$ applied to the entire line $(x, 0)\ x \in \mathbb{R}$. A new operator is constructed for each required output point along the line using the local velocity at the output point $v(x_0, \Delta z)$. The core assumption at the heart of the GPSPI method is its dependence on the fact that the wavefield at each output point $(x_0, \Delta z)$ is calculated by propagating the wavefield from the line at depth $z = 0$ assuming that the entire wavefield at depth $z = 0$ propagates through a medium of constant velocity $v(x_0, \Delta z)$. That is, the local region between the line $(x, 0)\ x \in \mathbb{R}$ and the point $(x_0, \Delta z)$ is assumed to be homogeneous. For this reason, equation (2) with symbol as defined in equation (3) is often referred to as the locally-homogeneous approximation (Fishman et al., 1997). The magnitude of Δz is typically on the order of $\sim 10m$, which is usually much smaller than the scale of the range velocity variation and so a range-homogeneous approximation is often reasonable.

The design of the v(z) operator

We will consider an operator that treats the case of a linear velocity in $v(z)$. Margrave (2001) extended Stolt's $f-k$ migration method to $v(z)$ using the methods of nonstationary filters. We will use a similar approach to extend the GPSPI operator to a linear $v(z)$.

In this case, the exponential terms in equation (3) may be replaced by integrations:

$$\exp\left(i\int_0^{\Delta z}\sqrt{\frac{\omega^2}{v(z')^2}-k_x^2}dz'\right) \tag{5}$$

for the $|k(x)| \leq \frac{\omega}{v(z')}$ case. This effectively uses a WKBJ approximation (see *eg* Aki and Richards, 2002), and so the operator can be considered a WKBJ operator.

Although velocity models of the earth may contain a vertical velocity gradient that can be approximated by a local linear gradient, this is not the reason for this approach. The advantage of this approach is that a velocity with positive gradient in z has the effect of limiting the aperture of the migration operator on the line $(x, 0)\ x \in \mathbb{R}$. This may be conceptualized by considering a point source at depth in a medium with a positive vertical velocity gradient. The raypaths leaving away from the point source in the upper hemisphere will all intersect the surface within a finite radius from the source.

In the original GPSPI algorithm, the operator must operate on the entire real line $x \in \mathbb{R}$. This is impossible in a numerical situation, so the operator that is calculated for a given frequency ω then must be truncated in either the x or k_x domain. In the case of an implementation in $\omega - k_x$ domain, as in the reference implementation of GPSPI, this truncation is frequently taken to include the entire extent of the k_x data available. In the

case of the FOCI implementation in the $\omega - x$ domain, this truncation is much shorter. The final operator width is frequently specified in terms of an odd number of "points", with the total width spanning the trace spacing multiplied by the number of points. The operator's radial extent is then calculated by subtracting one from the number of points, dividing by two, and multiplying by the trace spacing.

Recalling that the operator is a nonstationary filter, we recognize that this truncation will result in the Gibbs phenomenon. In $\omega - k_x$ as in the reference implementation of GPSPI, the truncation is the full width of the data, which does not lead to significant instability. In FOCI, however, where for performance reasons the truncation commonly occurs at only a few hundred meters radius (far less than the usual extent of the data), this leads to instability in the propagation, and great pains must be taken to correct this problem (see *eg* Margrave et al., 2004). The FOCI algorithm corrects for the introduced instability very well, and is an effective and rapid implementation of the GPSPI concepts. The algorithm works by first designing a truncated operator for propagation, and then using Wiener match filtering to stabilize the operator.

Due to its intrinsic natural self-truncation, this $v(z)$ approach allows the primary generation of a truncated operator that is inherently stable, and so it does not require the secondary stage of match-filtering for stabilization. Although there is a slight advantage to avoiding the stabilization in terms of numerical efficiency, the real advantage is due to the fact that FOCI cannot yet be practically used in 3D imaging. The 3D extension of FOCI requires the calculation of a 2D Wiener match filter, which is an extremely difficult calculation. Therefore, the $v(z)$ approach allows a much simpler extension to three dimensions by avoiding this computation. Additionally, it is somehow more intellectually pleasing to generate an inherently stable operator right at the beginning instead of generating an unstable operator and then working to stabilize it afterwards.

Choosing the v(z) parameters

For the choice of $v(z) = v_0 + Az$, two constraints are required to uniquely determine the velocity function. Since the $v(z)$ velocity function is purely conceptual, designed to stabilize the operator and not to represent any physical gradient, for our first constraint we require that the overall traveltime through the small depth step Δz through the $v(z)$ medium match the traveltime through the same depth step at the velocity model's local value v_{ref}. For our second constraint, we choose the gradient such that a ray with a takeoff angle of 90° at the output point is normally incident at the input depth at precisely the desired operator's aperture radius.

This leads us to two equations for the two unknowns. From raypath arguments (see *eg* Aki and Richards, 2002) it can be shown that, for an aperture radius x_0, a depth step of Δz, and an initial velocity v_0, the required gradient (accelerator) A is found:

$$A = \frac{2v_0\Delta z}{x_0^2 - \Delta z^2} \tag{6}$$

By equating the traveltimes for a linear $v(z)$ with a constant velocity medium at v_{ref}, the

second constraint is given in equation (7):

$$\log\left(1+\frac{A\Delta z}{v_0}\right)=\frac{A\Delta z}{v_{ref}} \tag{7}$$

From equation (6) it is obvious that the aperture x_0 must not approach Δz too closely, or a singularity results.

Combining equations (6) and (7) and solving for v_0 yields equation (8):

$$v_0 = v_{ref}\log\left(1+\frac{2\Delta z^2}{x_0^2-\Delta z^2}\right)\frac{(x_0^2-\Delta z^2)}{2\Delta z^2} \tag{8}$$

So with equations (6) and (8), the required $v(z)$ is expressed purely in terms of reference velocity v_{ref}, operator radius x_0 and depth-step size Δz.

The symbol

The resulting $v(z)$ symbol is similar to the GPSPI symbol in amplitude (Figure 1), and phase (Figure 2). The difference between the symbols is extremely small, but can be seen

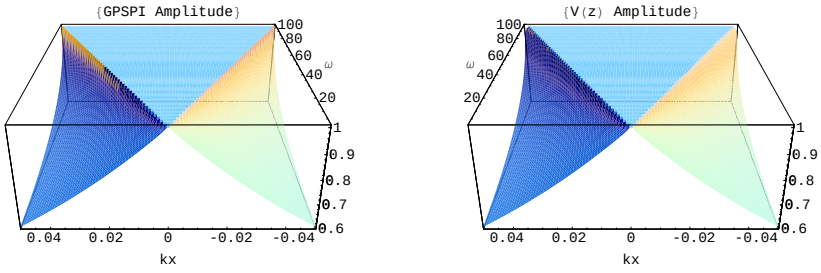

FIG. 1. Symbol amplitude for a homogeneous medium. GPSPI is shown on the left, and the $v(z)$ symbol is shown on the right. Aperture $x_0 = 50m, v_{ref} = 2000ms^{-1}, v_0 = 1921ms^{-1}, A = 16s^{-1}, dz = 10m$

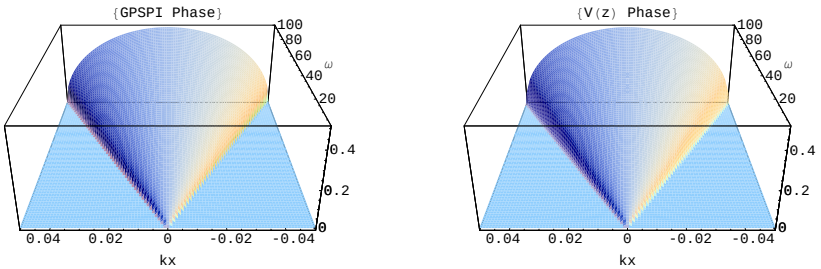

FIG. 2. Symbol phase for a homogeneous medium. GPSPI is shown on the left, and the $v(z)$ symbol is shown on the right. Aperture $x_0 = 50m, v_{ref} = 2000ms^{-1}, v_0 = 1921ms^{-1}, A = 16s^{-1}, dz = 10m$

in Figure 3.

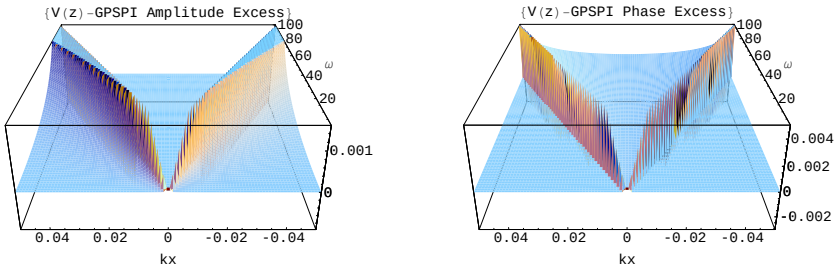

FIG. 3. Symbol differences, $v(z)$ minus GPSPI. Amplitude difference on the left, phase difference on the right.

The $\omega - x$ operator

The FOCI algorithm applies the operator within the $\omega - x$ domain. The $v(z)$ operator within this domain is shown in Figure 4, with $v(z)$ operators displayed in left hand panels, and equivalent FOCI panels on the right. The top panel of this display shows the real and imaginary parts of a single 31 point ($187.5m$) operator at frequency 70 Hz, for a depth step of $12.5m$, with design parameters $v_0 = 1869ms^{-1}$ and $A = 21s^{-1}$ for an effective aperture of $x_0 \approx 50m$. The second panel shows the full operator's amplitude spectrum transformed back into the $\omega - k_x$ domain, plus the operator raised to the power of 50. This exponentiation demonstrates the stability of the operator: when applied 50 times, the overall effect of the operator is to preserve the amplitude to nearly 1. The third panel demonstrates the phase of the operator in the $\omega - k_x$: it is very nearly the same as the desired ideal phase of the operator. The difference between the $v(z)$ operator and the FOCI operator is striking. The

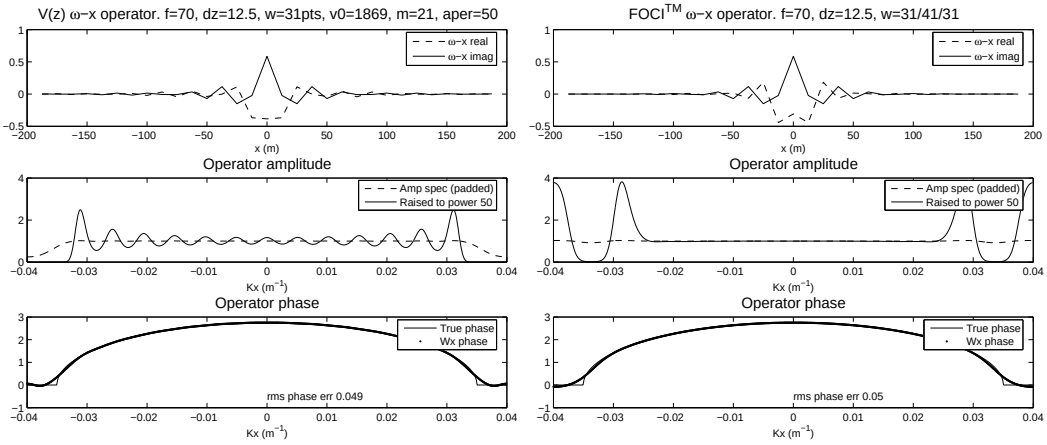

FIG. 4. In the left panel, the 31-pt ($187.5m$) $v(z)$ operator with $50m$ aperture in the $\omega - x$ domain and also transformed back into the $\omega - k_x$ domain. On the right, the same panel for the 31/41/31 ($187.5m$ final width) FOCI operator.

$v(z)$ operator has a very slight amount of controlled instability throughout its extent, while the FOCI operator is extremely stable in the centre. This FOCI operator was calculated with a 31 point forward operator, a 41 point inverse operator, and a 31 point ($187.5m$) final window. With a slightly more expensive calculation, it is possible to reduce FOCI's edge instabilities with a larger inverse operator length.

If the $v(z)$ aperture radius is reduced from $50m$ down to $30m$ and the same operator is recalculated, we expect that the stability should be improved, perhaps at the expense of the accuracy of the propagation at high wavenumbers. Figure 5 shows that this is indeed the case. There is also a slight difference in the phase. Near the evanescent boundary, the

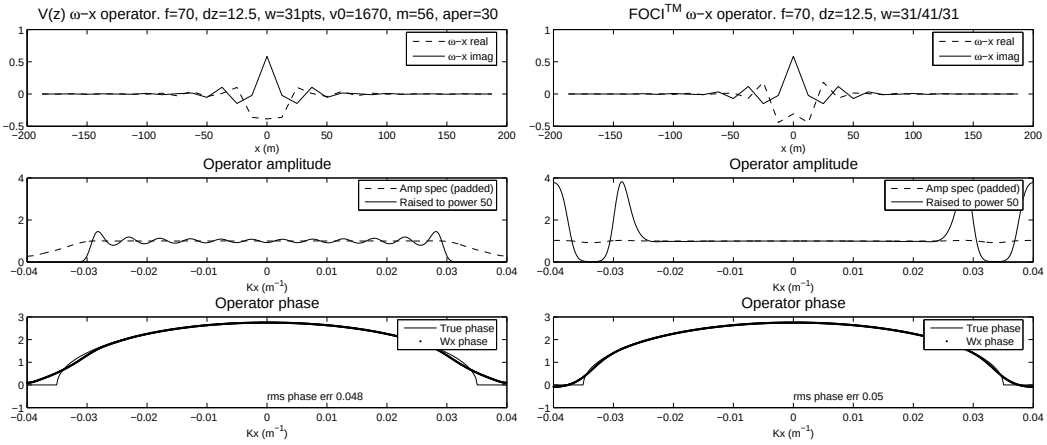

FIG. 5. In the left panel, the 31-pt ($187.5m$) $v(z)$ operator with $30m$ aperture in the $\omega - x$ domain and also transformed back into the $\omega - k_x$ domain. On the right, the same panel for the 31/41/31 ($187.5m$ final width) FOCI operator.

phase error increases as the aperture is reduced. This is no surprise, as the wavefield near the evanscent boundary will be coming into the output point from near the aperture radius at the input depth plane. The $v(z)$ process implicitly bends these raypaths, leading to phase error. However, from the amplitude spectrum it can be seen that this region of incorrect phase will be heavily rejected anyway.

It is interesting to note that the $v(z)$ operator still contains a noticeable amount of ripple throughout its extent. Yet as will be shown later on, these operators can be successfully used to migrate data through hundreds of steps.

TESTING

The $v(z)$ symbol was implemented within both the reference GPSPI and FOCI frameworks, using existing MATLAB codes developed by CREWES and POTSI. Impulse response and focussing-power tests were calculated using explicit GPSPI methods, while full prestack depth migrations were calculated using FOCI-derived algorithms.

Impulse response

The impulse response of the $v(z)$ operator in a homogenous medium is compared to the standard square-root of GPSPI in Figure 6. These operators were designed for a depth step of $200m$. The $v(z)$ response is spatially limited compared to the standard GPSPI response. It can be seen that the arms of the $v(z)$ response taper off in strength faster than the arms of the GPSPI response. This is especially evident in the response of the operator with the very narrow ($300m$ width compared to a $200m$ depth step) aperture width, though it is also

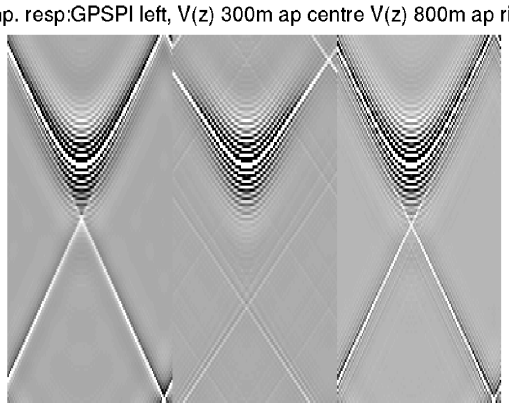

FIG. 6. Impulse response of standard GPSPI operator on the left compared to the $v(z)$ operator with a 300m aperture in the middle, and a $v(z)$ operator with a 800m aperture on the right. Both symbols propagated an impulse 200m through a homogeneous medium.

visible in the response of the wider ($800m$) aperture.

The narrow-aperture impulse response also appears to have a significantly different position at the outer ends of the arms. This is undoubtedly due to the strong velocity gradients that are used to truncate the operator and the resulting phase errors. This effect is much less noticeable on the arms of the wide-aperture response.

Focussing power

The focussing power of an operator measures its ability to return a forward-propagated wavefield back to its initial impulsive source. Focussing power tests were performed on a homogeneous velocity model and on an inhomogeneous velocity model. For all focussing power tests, the operator width used was effectively the width of the entire data set, due to the use of the GPSPI reference implementation.

Homogenous focussing

The focussing power of the regular GPSPI operator through a homogeneous medium of $2500ms^{-1}$ is compared to that of the $v(z)$ operator in Figure 7. In this case, the $v(z)$ operators used $15m$ and $40m$ aperture widths. The relative energy density measured as a function of radius from the centre of the response (*ie* the "pointiness" of the result) is also shown in Figure 7. The relative energy densities of the GPSPI and $v(z)$ $40m$ operators are virtually indistinguishable, while the $v(z)$ $15m$ operator result is clearly severely defocussed. Since the chosen depth step for these operators was $10m$, it is clear that the operator aperture must be significantly larger than the depth step to perform well.

Inhomogeneous focussing

To investigate the $v(z)$ operator in a less trivial medium, the focussing power of the regular GPSPI operator through an inhomogeneous medium (in this case, a vertically-

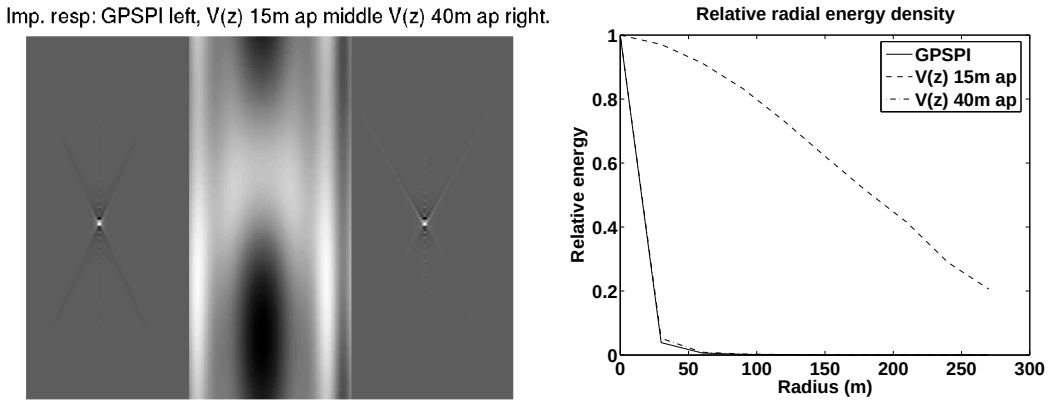

FIG. 7. Focussing power through a homogeneous medium, 10 steps of $10m$ through $2500ms^{-1}$. In the left panel, focussing power of the GPSPI (left) vs. that of the $v(z)$ $15m$ aperture-width operator (centre) and the $v(z)$ $40m$ aperture-width operator (right). In the right panel, relative energy density of the GPSPI and $v(z)$ operators is plotted.

homogeneous $4500ms^{-1}$ region sandwiched between two vertically-homogeneous $1500ms^{-1}$ regions) is compared to that of the $v(z)$ operator in Figure 8. As before, the $v(z)$ operators used $15m$ and $40m$ aperture widths. The relative energy density measured as a function of radius from the centre of the response is also plotted in Figure 8. Again, we see strong

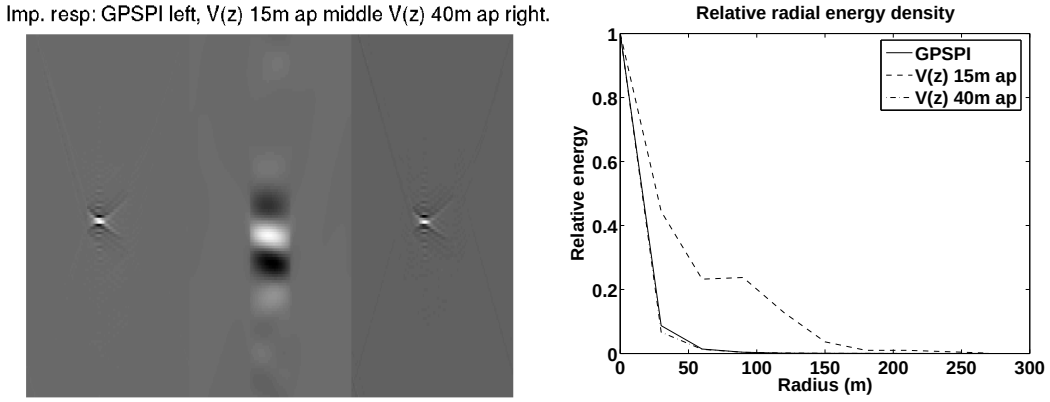

FIG. 8. In the left panel, focussing power of the GPSPI (left) vs. that of the $v(z)$ $400m$ aperture-width operator (right). In the right panel, relative energy density of the GPSPI and $v(z)$ operators is plotted.

agreement between GPSPI and $v(z)$ as long as the aperture window is large with respect to the depth step.

Marmousi migration

In addition to impulse response and focussing power tests, full pre-stack migrations of the Marmousi model were calculated using FOCI. The standard FOCI operator was compared to a modified version that included the $v(z)$ symbol in the operator design phase but was otherwise identical in all operational parameters.

A pre-stack migration image of the Marmousi model was generated, using both standard FOCI (Figure 9) and $v(z)$ (Figure 10) operators.

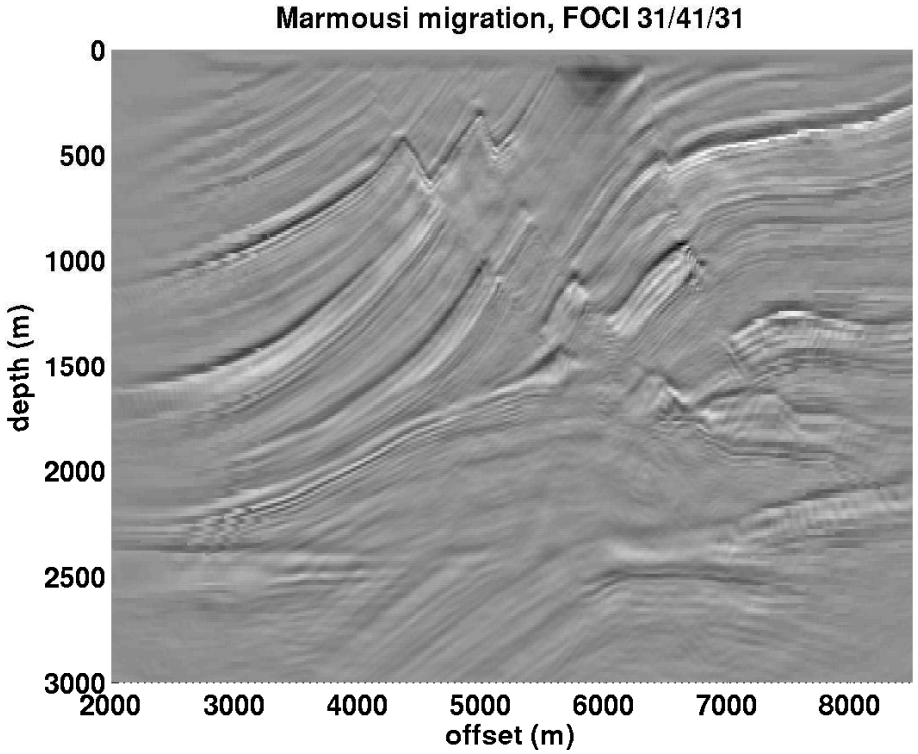

FIG. 9. Marmousi image, FOCI migration with full stabilization. (31 point forward operator, 41 point inverse operator, 31 point final window, $187.5m$ effective operator width.)

Several subsections of the image are compared more closely in Figures 11–14. Each figure contains four panels. On the top left, the $v(z)$ image is displayed. On the bottom left, the FOCI image is displayed. On the top right, the corresponding region from the Marmousi velocity model is displayed. On the bottom right, a histogram of the colourbar usage of both images is shown, in order to allow for an accurate comparison of the relative strengths and weaknesses of amplitudes within the images.

In region 1 (Figure 11) the complex layering is clearly imaged by both algorithms. It is difficult to choose a "better" image, though in several cases (*eg* near (3600, 1300) and (4400, 1000)) the $v(z)$ image seems to have better continuity of the reflectors. In region 2 (Figure 12) the images are slightly different. The $v(z)$ image seems to display better reflector continuity, but in some cases loses some of the sharpness of the FOCI image. In region 3 (Figure 13) again, the $v(z)$ image seems to have better continuity. Also, the fault line appears more obviously in the $v(z)$ image. Finally, in region 4 (Figure 14), the reservoir target area is displayed. This reservoir target is well-imaged by both algorithms. The $v(z)$ image appears to have less noise contamination than the FOCI image. This is especially evident in the top-right corner of each region, around (7500, 2250), though it may be observed throughout the region.

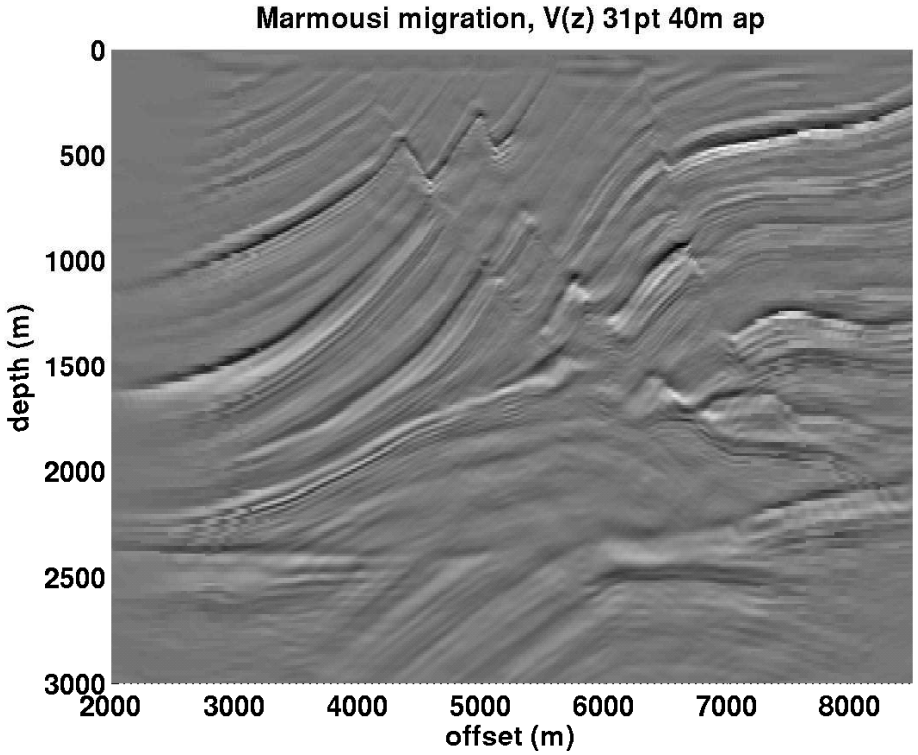

FIG. 10. Marmousi image, $v(z)$ migration. (31 point ($187.5m$) operator, $40m$ aperture radius.)

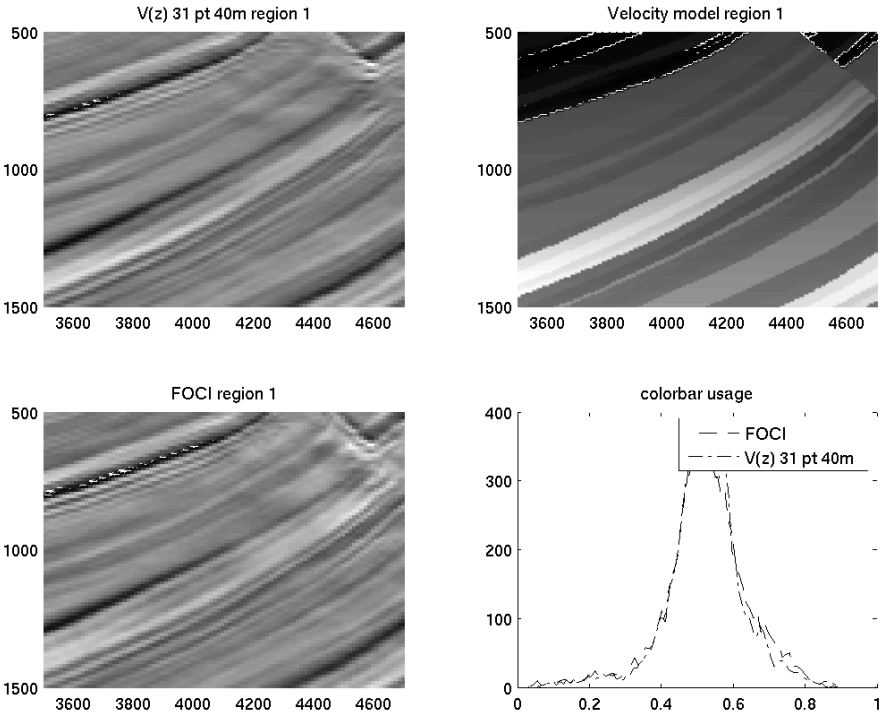

FIG. 11. Marmousi region 1

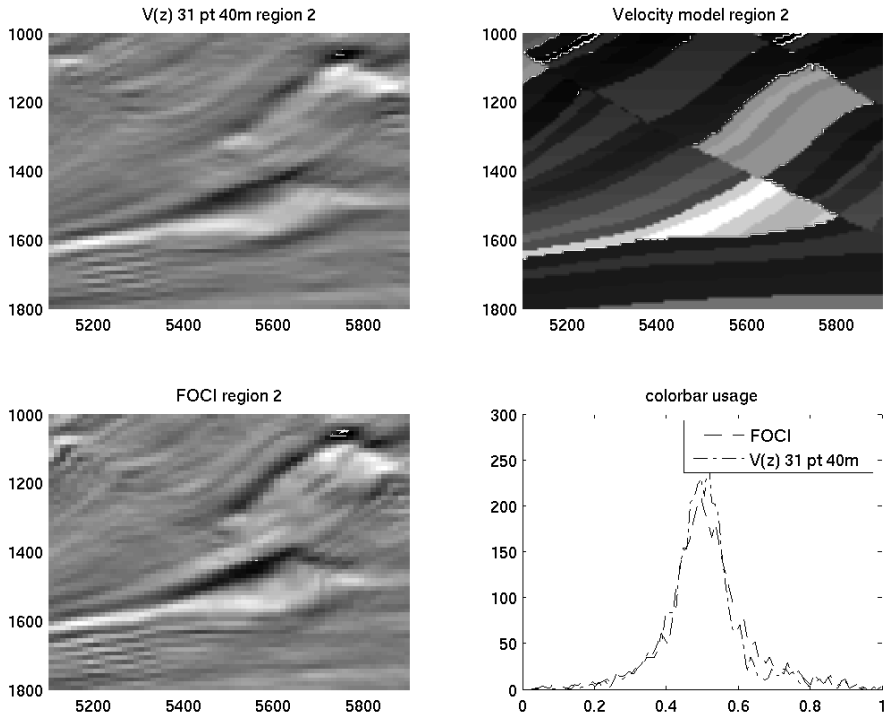

FIG. 12. Marmousi region 2

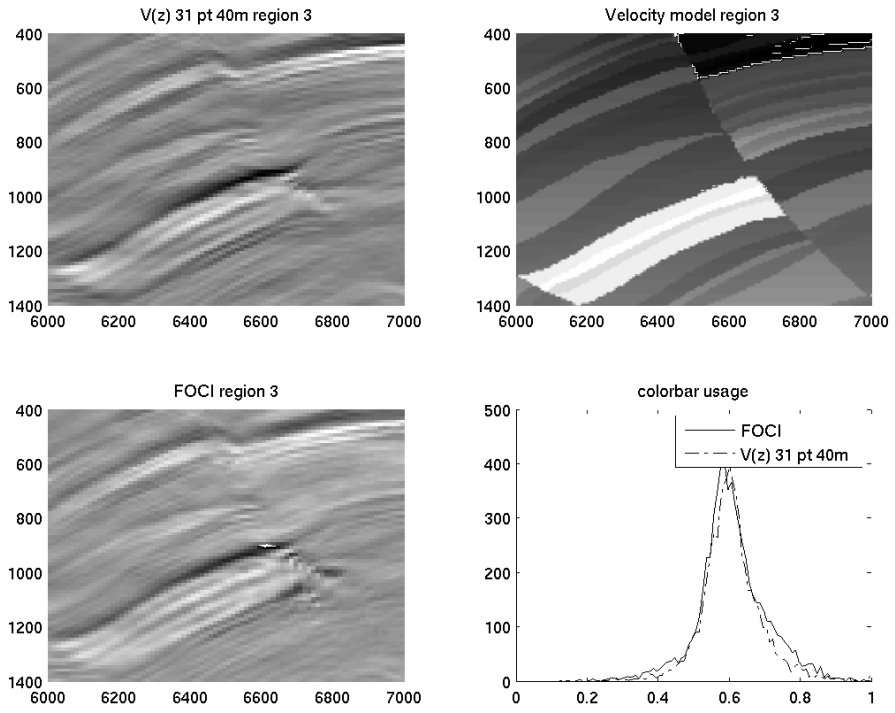

FIG. 13. Marmousi region 3

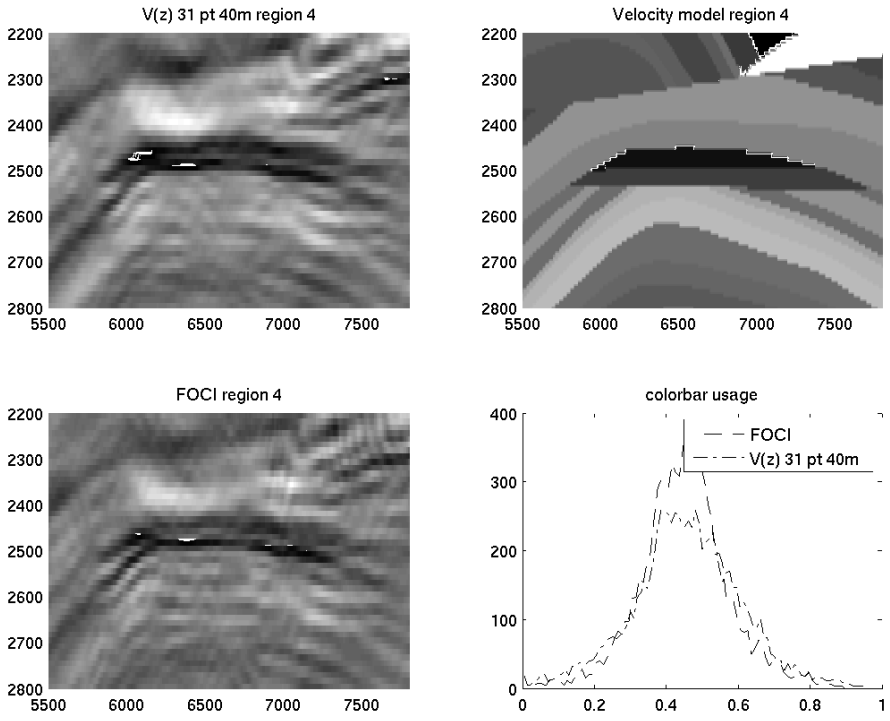

FIG. 14. Marmousi region 4

Parameter choice and performance

The primary factor in choosing parameters for the operation of the $v(z)$ operator is time-to-compute vs. image quality. Simply put, more points mean a better image, but more points mean a slower calculation. In Figure 15, another $v(z)$ Marmousi image with a 101 point ($625m$) operator and an $80m$ aperture is shown. All calculations were performed using MATLAB 7.1 on Linux-based PC computers with 3.06 GHz Intel Pentium 4 CPUs. The 31 point ($187.5m$) operator requires approximately 4 minutes per shot record to migrate, resulting in a total time of about 16 hours. The 101 point operator requires approximately 4.6 minutes to calculate each shot record, with a total time of slightly more than 18 hours. As can be seen from a careful examination of Figures 10 and 15, the 101 point operator does result in small improvements in the quality of the final image. These improvements were gained at the cost of an extra 15% calculation time.

Aperture radius does not affect calculation time. It does, however, affect the quality of the image if the radius is not significantly larger than the depth step of each extrapolation. Also, the stabilization of the operator is ineffective if the radius is not significantly less than the radial extent of the operator. In the Marmousi data set, traces are $12.5m$ apart. Thus, a 31 point operator has an effective radial extent of $15 \times 12.5m = 187.5m$. Therefore, the choice of a $40m$ aperture radius is smaller than the radial extent of the operator ($187.5m$), but greater than the depth step of the extrapolation ($12.5m$).

Testing suggests that a useful aperture width measure is such that the ratio of operator

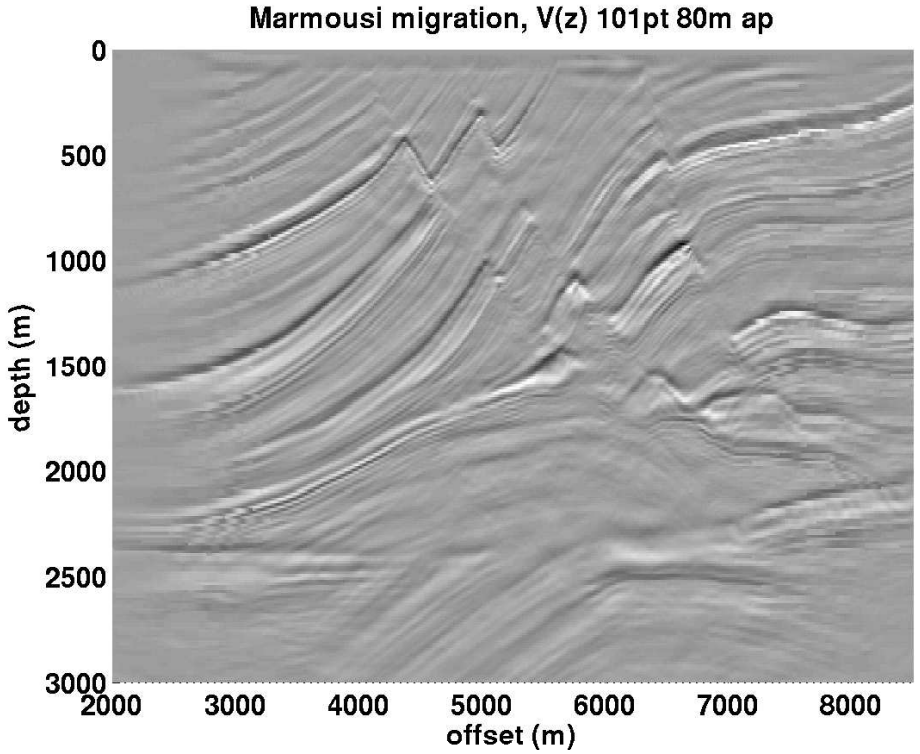

FIG. 15. Marmousi image, $v(z)$ migration. (101 point ($625m$) operator, $80m$ aperture radius.)

radial extent to aperture radius is somewhat greater than the ratio of aperture radius to depth-step size. Dividing these two ratios and calling the quotient ρ:

$$\left(\frac{dx(OW-1)/2}{x_0}\right)\left(\frac{dz}{x_0}\right) = \rho \tag{9}$$

allows a numerical description of the aperture radius x_0 where OW is the operator width in points, dx is trace spacing in meters, and dz is depth-step size in meters.. Therefore, aperture radius x_0 may be suggested as follows, given that useful values of this ratio are in the range $\rho = (1, 2.5]$. Solving equation (9) for aperture:

$$x_0 = \sqrt{\frac{dxdz(OW-1)}{2\rho}} \tag{10}$$

This aperture radius balances the requirement for effective natural truncation of the operator to avoid Gibbs phenomenon instability, while maximizing the quality of the final image. The stability factor ρ allows the processor to tune the image quality and stability as necessary for any given situation.

CONCLUSIONS

Replacing the usual GPSPI square-root symbol exponential as in equation (3) with an exponential that is an integral involving a linear velocity over depth as in equation (5) results in an operator symbol that may be used directly in any GPSPI-derived algorithm including the high-performance FOCI algorithm.

Although the operator appears not to look as perfectly flat as FOCI-generated operators within the bulk of the wavelike region, it nonetheless results in stable and accurate images. The $v(z)$ operator naturally and effectively truncates the extrapolation operator in the $\omega - x$ domain, and therefore obviates the need for the FOCI stabilization step. Although this does save a trivial amount of computation time, the true benefit is that a clear path towards a high-performance 3D algorithm based on these principles has been revealed.

REFERENCES

Aki, K., and Richards, P. G., 2002, Quantitative Seismology: University Science Books, second edn.

Fishman, L., Gautesen, A. K., and Sun, Z., 1997, Uniform high-frequency approximations of the square root Helmholtz operator symbol: Wave Motion, **26**, 127–161.

Gazdag, J., 1978, Wave equation migration with the phase-shift method: Geophysics, **43**, No. 7, 1342–1556.

Gazdag, J., and Sguazzero, P., 1984, Migration of seismic data by phase shift plus interpolation: Geophysics, **49**, No. 2, 124–131.

Hörmander, L., 1985, The Analysis of Linear Partial Differential Operators, vol. 1-4: Springer.

Margrave, G. F., 1998, Theory of nonstationary linear filtering in the Fourier domain with application to time-variant filtering: Geophysics, **63**, No. 1, 244–259.

Margrave, G. F., 2001, Direct Fourier migration for vertical velocity variations: Geophysics, **66**, No. 5, 1504–1514.

Margrave, G. F., Al-Saleh, S. M., Geiger, H. D., and Lamoureux, M. P., 2004, The FOCI algorithm for seismic depth migration, Tech. rep., CREWES Research Report.

Margrave, G. F., and Ferguson, R. J., 1999, Wavefield extrapolation by nonstationary phase shift: Geophysics, **64**, No. 4, 1067–1078.